Characterization of the Low-Mass Members in the Praesepe Star Cluster

P. F. Wang[1] W. P. Chen[1,2], C. C. Lin[2], A. K. Pandey[3], C. K. Huang[2], N. Panwar[2], C. H. Lee[2], J. K. Guo[2], B. Goldman[4], M. F. Tsai[5] W. S. Burgett[6], K. C. Chambers[6], P. Draper[7], H. Flewelling[6], T. Grav[8], J. N. Heasley[6], K. W. Hodapp[6], M. E. Huber[6], R. Jedicke[6], N. Kaiser[6], R.-P. Kudritzki[6], G. A. Luppino[6], R. H. Lupton[9], E. A. Magnier[6], N. Metcalfe[7], D. G. Monet[10], J. S. Morgan[6], P. M. Onaka[6], P. A. Price[6], C. W. Stubbs[11], W. Sweeney[6], J. L. Tonry[6], R. J. Wainscoat[6]. C. Waters[6],

Received _____; accepted _____

[1]Department of Physics, National Central University, 300 Jhongda Road, Jhongli 32001, Taiwan

[2]Graduate Institute of Astronomy, National Central University, 300 Jhongda Road, Jhongli 32001, Taiwan

[3]Aryabhatta Research Institute of Observational Sciences, India

[4]Max Planck Institute for Astronomy, Königstuhl 17, D-69117 Heidelberg, Germany

[5]Depart of Computer Science and Information Engineering, national Central University, 300 Jhongda Road, Jhongli 32001, Taiwan

[6]Institute for Astronomy, University of Hawaii, 2680 Woodlawn Drive, Honolulu HI 96822

[7]Department of Physics, Durham University, South Road, Durham DH1 3LE, UK

[8]Department of Physics and Astronomy, Johns Hopkins University, 3400 North Charles Street, Baltimore, MD 21218, USA

[9]Department of Astrophysical Sciences, Princeton University, Princeton, NJ 08544, USA

[10]US Naval Observatory, Flagstaff Station, Flagstaff, AZ 86001, USA

[11]Department of Physics, Harvard University, Cambridge, MA 02138, USA

ABSTRACT

Membership identification is the first step to determine the properties of a star cluster. Low-mass members in particular could be used to trace the dynamical history — mass segregation, stellar evaporation, tidal stripping — of a star cluster in its Galactic environment. We present member candidates above the hydrogen burning limit, $\lesssim 0.1$ $M_{\odot}$, of the nearby Praesepe cluster (M 44), by using the 2MASS and Pan-STARRS photometry, and the PPMXL proper motions, from which a total of 1040 member candidates have been identified, 872 of which should be highly probable members. The cluster is found to have a binary frequency of 20–30%, with a high occurrence of similar mass pairs. Some member candidates found in previous studies have proper motions inconsistent with membership, so should be excluded. The mass function shows a deficit of members below 0.3 solar masses. Mass segregation is clearly evidenced, and the lowest-mass member stars are being evaporated in this mid-aged (890 Myr), disintegrating cluster.

Subject headings: proper motions – stars: evolution – stars: mass function — open clusters and associations: individual (Praesepe) – infrared: stars

1. Introduction

A star cluster manifests itself as a density concentration of comoving stars in space. Born out of the same molecular cloud, the member stars have roughly the same age, similar chemical composition, and at essentially the same distance from us. Star clusters, therefore, serve as good test beds to study stellar formation and evolution. In order to diagnose the properties of a star cluster, such as its age, distance, size, spatial distribution, and mass function, etc., it is necessary to identify as completely as possible the member stars. In particular, with a sample of members including the lowest mass stars, or even substellar objects, one could trace the dynamical history of an open cluster, like the mass segregation, stellar evaporation, and tidal stripping in the Galactic environment.

The nearby Galactic open clusters are useful in study of their low-mass population. Praesepe (M 44; NGC 2632; the Beehive Cluster) is such a rich ($\sim$ 1000 members) and intermediate-age (890 Myr Marigo et al. 2008) stellar aggregation in Cancer, as a system of the Hyades moving group (Eggen 1960). Compared to Praesepe, the Hyades cluster itself has a scattered main sequence (MS) in the color-magnitude diagram (CMD) because of the significant depth with respect to its distance. The advantages of studying stars in Praesepe are numerous. First, the distance is close enough to detect low-mass stars and brown dwarfs (BDs). Second, the proper motion (PM) of the cluster is distinct from that of the field stars, as seen in Figure 1, so contamination is minimized when characterizing the cluster. Third, in contrast to a star cluster at birth for which the spatial distribution of member stars is dictated by the parental cloud structure, the distribution of members in an intermediated-age cluster such as Praesepe depends mainly on the interaction between members, from which we could investigate the dynamical evolution of the cluster.

Stellar membership of Praesepe has been surveyed with photometry and astrometry. Klein-Wassink (1927) used PMs to identify bright members within a 1-deg radius of the

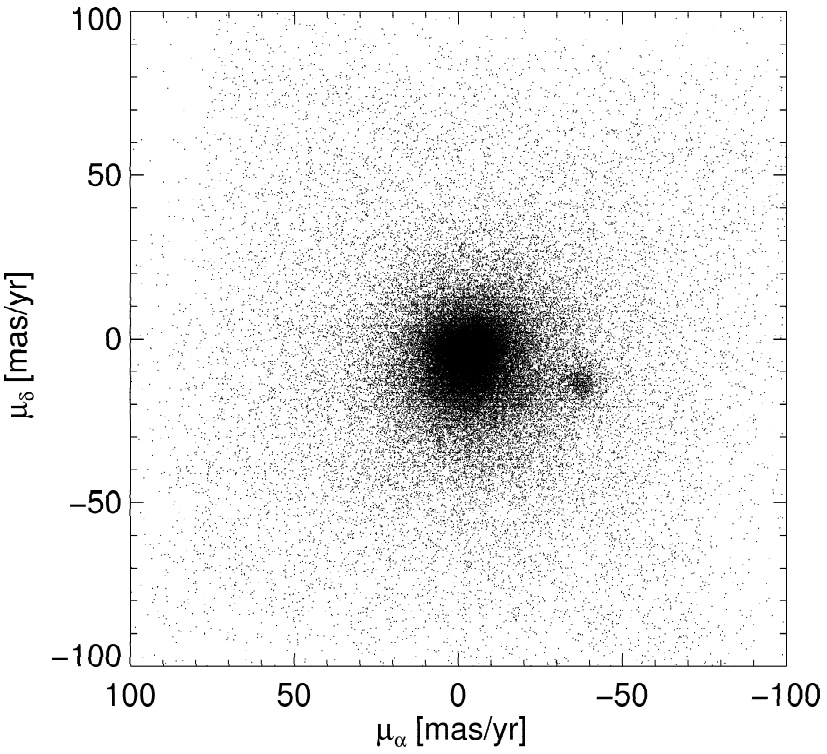

Fig. 1.— The PPMXL proper motion vector point diagram of stars toward Praesepe. Only stars spatially within the the central 2° are shown for clarity. In addition to the central concentration ($\mu_{\rm RA} = -4$ mas yr^{-1}, and $\mu_{\rm Ded} = -3$ mas yr-1) showing the relative motion of field stars respect to the Sun, there is a distinct secondary peak around $\mu_{\rm RA} = -35$ mas yr^{-1}, and $\mu_{\rm Dec} = -13$ mas yr^{-1} due to the cluster.

cluster center. Jones & Cudworth (1983) extended the study to include intermediate-mass stars to a detection limit of $V \sim 17$ mag. With PMs and photometry, Jones & Stauffer (1991) identified a list of member candidates from $V \sim 9$ to 18 mag within 2° of the cluster center. By using red sensitive emulsions which are suitable to observe red, low-mass stars, Hambly et al. (1995a) carried the magnitude limit down to $R \gtrsim 20$ mag, thereby pushing the mass limit of member stars to ~ 0.1 $M_\odot$. On the basis of this sample, these authors then derived a rising mass function toward the low-mass end, and presented evidence of mass segregation (Hambly et al. 1995b). With sky survey databases, Adams et al. (2002) examined a sky area of 100 deg^2 by combining the near-infrared (NIR) Two Micron All Sky Survey (2MASS) and Palomar Observatory Sky Survey plates digitized by the USNO to extend the lower MS of the cluster down to 0.1 $M_\odot$, and determined the radial density profile of member stars. A comprehensive study later was done by Kraus & Hillenbrand (2007), who surveyed a sky area of 300 deg^2 to identify members by spectral energy distribution of photometry in eight optical to infrared bands ($ugrizJHK$) taken from the Sloan Digital Sky Survey (SDSS) and 2MASS. In addition, the PM data were taken from the UCAC2 for bright stars or calculated from USNO-B and SDSS positions. The sample of Kraus & Hillenbrand (2007) covered a range of spectral types, F0–M5, almost reaching the BD regime. For early-type stars, the incompleteness resulted from the bright limit of the UCAC2, whereas for later-type members the incompleteness was caused by the detection limits of the USNO-B and 2MASS.

There have been efforts to identify BDs in Praesepe. Pinfield et al. (1997) covered one deg^2 down to $I \sim 21$ mag and identified 19 BD candidates without spectral confirmation. Chappelle et al. (2005) presented deep optical and NIR observations covering 2.6 deg^2 down to 0.06 $M_\odot$. González-García et al. (2006) explored the central 0.6 deg radius region, reaching a detection limit of $i_{\rm SDSS} \sim 24.5$ mag corresponding to ~ 0.05–0.13 $M_\odot$, and identified one substellar candidate. Boudreault et al. (2010) performed an optical

I_c band and NIR J and K_s band photometric survey covering 3.1 deg^2 with detection limits of $I_c \sim 23.4$ mag and $J \sim 20.0$ mag, and found a handful of substellar candidates. These authors also found a rising mass function until 0.1 $M_\odot$, in contrast to the Hyades which have about the same age as Praesepe but are deficient of very low-mass stars and BDs. Possible explanations include different initial mass functions for the two clusters, or Praesepe somehow did not experience as much dynamical perturbation in its environments (Bouvier et al. 2008). A recent study with the UKIRT Infrared Deep Sky Survey (UKIDSS) Galactic Clusters Survey, however, has found a declining mass function toward lower masses (Boudreault et al. 2012).

As a star cluster ages, gravitational scattering due to stellar encounters results in mass segregation (Spitzer & Shull 1975); that is, massive stars tend to concentrate toward the center of the cluster, whereas lower mass stars, with a greater velocity dispersion, are distributed out to greater radii. For Praesepe, Hambly et al. (1995a) combined their observations, complete to $R \sim 20.0$ mag and $I \sim 18.2$ mag, with those of Mermilliod et al. (1990) with $I \lesssim 12$ mag, and showed a clear mass segregation effect. Using N-body simulations, de La Fuente Marcos & de La Fuente Marcos (2000) reported that the probability of finding a BD in an open cluster is almost the same over the whole cluster area because BDs are distributed quite uniformly even at late stages of the cluster evolution. These authors simulated the dynamical evolution of substellar population in open clusters and suggested that BDs in clusters escape preferentially by evaporation.

Previous studies either were significantly deep but limited in sky coverage, or covered wide areas but were restricted to only brighter (more massive) members. Studies with large sky coverage often identify cluster membership on the basis of photometry, and PM measurements for faint members are lacking. For example, the UCAC3 has a limiting magnitude of $R \sim 16$ mag. In this paper, we present photometric (2MASS and

Pan-STARRS) and astrometric (PPMXL) diagnostics to select the member candidates in Praesepe. Our sample allows us to identify and characterize members near the hydrogen burning limit to investigate their mass function and the segregation effect. We describe the photometric and PM data in Section 2, and how we identified probable members in Section 3. The discussion is in Section 4, for which we compare our results with those in the literature. The binarity is discussed, and evidence of mass segregation and tidal stripping is presented. The paper ends with a short summary as Section 5.

2. Data and Analysis

Data used in this study include photometry and PM information within a 5-deg radius around the Praesepe center (R.A.=$08^{\rm h}40^{\rm m}$, Decl.=$+19°42'$, J2000). The archival data were taken from the 2MASS Point Sources Catalog, PPMXL, and Pan-STARRS. The 2MASS Point Source Catalog (Cutri et al. 2003) has the 10σ detection limits of $J \sim 15.8$ mag, $H \sim 15.1$ mag, and $K_s \sim 14.3$ mag, and saturates around $J \sim 9$ mag, $H \sim 8.5$ mag, and $K_s \sim 8$ mag. The typical astrometric accuracy for the brightest unsaturated sources is about 70–80 mas. PPMXL is an all-sky merged catalog based on the USNO-B1 of positions, PMs, and optical and 2MASS photometry of 900 million stars and galaxies, reaching a limiting $V \sim 20$ mag (Roeser et al. 2010). The typical error is better than 2 milliarcseconds (mas) per year for the brightest stars with Tycho-2 (Høg et al. 2000) observations and more than 10 mas $\rm yr^{-1}$ at the faint limit.

Pan-STARRS (the Panoramic Survey Telescope And Rapid Response System) is a wide field (7 $\rm deg^2$) imaging system, with a 1.8 m, f/4.4 telescope (Hodapp et al. 2004), equipped with a 1.4 giga-pixel camera (Tonry et al. 2008). The prototype (PS1), located atop Haleakala, Maui, USA (Kaiser et al. 2010), has been patrolling the entire sky north of $-30°$ declination since mid-2010. Repeated observations of the same patch of sky with

a combination of $g_{\rm P1}$, $r_{\rm P1}$, $i_{\rm P1}$, $z_{\rm P1}$, and $y_{\rm P1}$ bands several times a month produce a huge inventory of celestial objects that vary in brightness or in position. Deep static sky images and catalog of stars and galaxies are also obtained. The PS1 filters differ slightly from those of the SDSS (Abazajian et al. 2009). The $g_{\rm P1}$ filter extends 20 nm redward of $g_{\rm SDSS}$ for greater sensitivity and lower systematics for photometric redshift estimates. SDSS has no corresponding y filter (Tonry et al. 2012). The limiting magnitudes are $g_{\rm P1} \sim 22.5$ mag, $r_{\rm P1} \sim 22$ mag, $i_{\rm P1} \sim 21.5$ mag, $z_{\rm P1} \sim 21$ mag, and $y_{\rm P1} \sim 19.5$ mag, with the saturation limit of ~ 14 mag. Upon completion of its 3.5 year mission by the end of 2013, PS1 will provide reliable photometry and astrometry. While incremental photometry of PS1 is available at the moment, the calibration of astrometry, hence the PM measurements, will need to tie down the entire sky, so no PS1 PM data were used here. In our study, we therefore made use of the 2MASS photometry for stars too bright for PS1, plus the PS1 photometry for faint stars, and the PPMXL PMs to select and characterize stellar member candidates.

3. Candidate Selection

Members in a star cluster are grouped in a six-dimensional parameter space, three in position (sky position and distance) and three in space motion (PM and radial velocity). The distance criterion often renders photometric identification of stars following the color-magnitude isochrone appropriate for the cluster. Our membership diagnosis relies on (1) grouping in sky position, (2) grouping in PMs, and (3) following the isochrones in the infrared and optical color-magnitude diagrams (CMDs). Our criteria hence should be more complete and reliable than the photometric selection alone.

The identification proceeds in an iterative way. The sources with 2MASS photometric uncertainties greater than 0.05 mag, roughly reaching $J \sim 15.2$ mag, $H \sim 14.6$ mag, and $K_s \sim 14.5$ mag, were removed from the sample. Candidacy was further winnowed in the J

versus $J - K_s$ CMD by including only objects with $J - K_s$ colors within 0.3 mag from the Padova theoretical isochrones (Marigo et al. 2008) for 890 Myr. This initial, wide range of color allowed us not to adopt an *a priori* stellar evolutionary model, but in turn to put different models to test, as demonstrated below.

With the initial photometric sample, we then identified stars with PMs close to that of the cluster, that is, to distinguish member candidates from field stars in Figure 1. Stars having PM values within a certain range of mas yr^{-1} of that of the cluster were selected. Obviously the choice of this range is a compromise between the quantity and the quality of the candidate list. The optimal range was decided by how the cluster grouping is blended with the field.

The PM distribution has two peaks, one for the cluster ($\mu_{\rm RA} \approx -36.5$ mas yr^{-1}, $\mu_{\rm Dec} \approx -13.5$ mas yr^{-1}) and the other for field stars ($\mu_{\rm RA} \approx -4$ mas yr^{-1}, $\mu_{\rm Dec} \approx -3$ mas yr^{-1}). The latter is the reflex Galactic motion of the Sun along this particular line of sight. The average PM we adopted for the cluster is close to those listed on SIMBAD, $\mu_{\rm RA} \approx -35.99 \pm 0.14$ mas yr^{-1}, $\mu_{\rm Dec} \approx -12.92 \pm 0.14$ mas yr^{-1} (Loktin & Beshenov 2003). Naturally, around the peak of the cluster, the distribution is dominated by members, and away from the peak the contamination by field stars becomes prominent. In fact, Praesepe is among a few cases (along with, for example, NGC 752) where the cluster's motion is clearly separated from that of the field, so the PM distribution exhibits a distinct secondary peak for the cluster. Most clusters otherwise have their PMs mixed with those of the field.

We exercised two levels of PM diagnosis. First, a Gaussian function was fitted to the secondary (cluster) peak. Even through the distribution is known to be non-Gaussian (Girard et al. 1989), the top part of the peak can still be approximated by a Gaussian with a standard deviation of 9 mas yr^{-1}. This is the PM range, namely within the radius $r_{\rm PM} = 9$ mas yr^{-1} of the cluster's PM, that we adopted to select PM membership among

the photometric candidates. This range is similar to what has been used by Kraus & Hillenbrand (2007) (8 mas yr^{-1}, the 2σ value for an M4 member in their sample) or by Boudreault et al. (2012) (8 mas yr^{-1} in $\mu_{\rm RA}$ and 12 mas yr^{-1} in $\mu_{\rm Dec}$) for membership selection. We note that Boudreault et al. (2012) derived, using relative PMs on the basis of the UKIDDS data, a different mean motion ($\mu_{\rm RA} = -34.17 \pm 2.74$, $\mu_{\rm Dec} = -7.36 \pm 4.17$). The discrepancy may arise because these authors used the medium value to choose the center of the PM range, yet the distribution is skewed because of the field. The next level of PM selection is $r_{\rm PM} = 4$ mas yr^{-1}, at which there is about the same contribution from the cluster and from the field, i.e., a 50% contamination of the sample. Figure 2 compares the cases of 4 versus 9 mas yr^{-1}. While bright candidates, including giant stars, are not much affected by the choice, the cluster sequence clearly stands out with the narrower PM range even without restrictions on position, color, or magnitude. The adoption of $r_{\rm PM} = 9$ mas yr^{-1} facilitates comparison between our results and previous works. But the $r_{\rm PM} < 4$ mas yr^{-1} sample is still kept for a more reliable selection of candidates. Figure 2 also shows the PM distribution along the line connecting the peak of the field and the peak of the cluster. Even with this projection showing the maximum distinction between the two peaks, the PM of the cluster is simply overwhelmed by that of the field.

We are now ready to finetune the photometric criteria. Figure 3a compares the J versus $J - K_s$ observations with model isochrones by Baraffe et al. (1998) (BCAH), Siess et al. (2000), Padova (Marigo et al. 2008), and Kraus & Hillenbrand (2007) (KH). To convert the effective temperature in the Siess et al. (2000) models to J, H, and K_s magnitudes, we made use of the table presented in Kenyon & Hartmann (1995). While all isochrones follow roughly each other for masses greater than ~ 0.7 M$_\odot$, they differ noticeably for low masses. The Padova isochrone is too blue to fit the data, and so is the BCAH isochrone. This cannot be caused by reddening because Praesepe is very nearby and the measured reddening $E(B-V)$ is merely 0.027 mag (Taylor 2006). Both the Siess and KH isochrones,

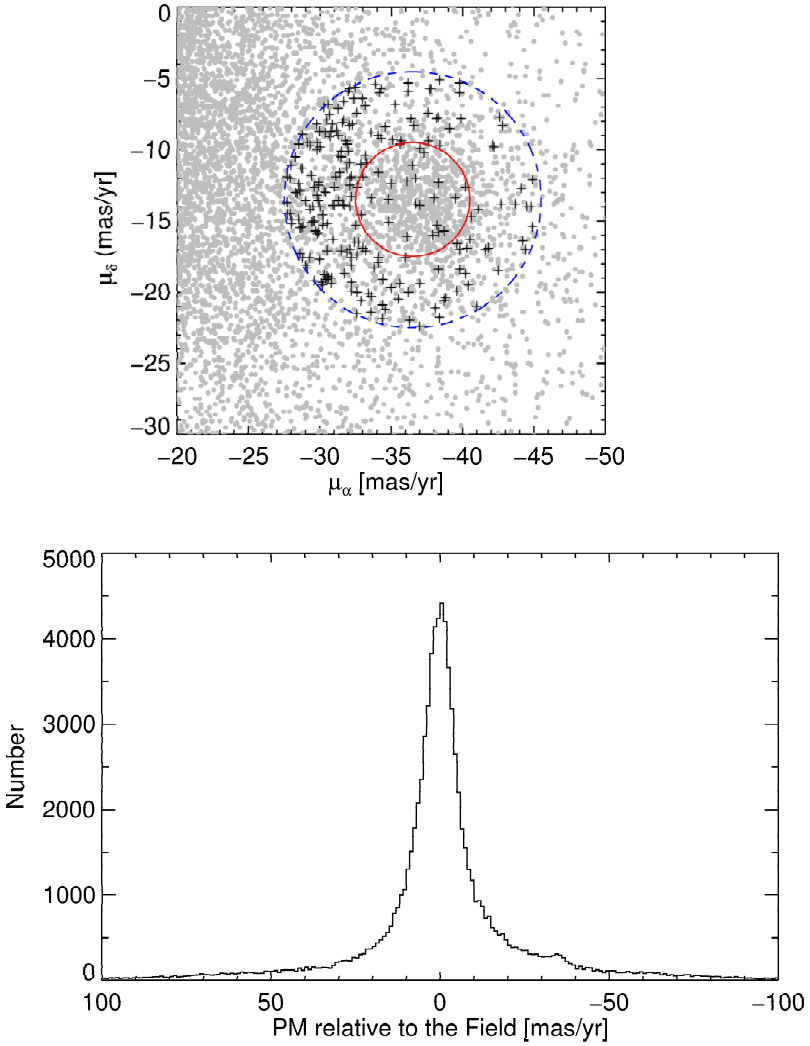

Fig. 2.— The 2MASS stars toward Praesepe. (a) The proper motion distribution. The two circles illustrate the radii of 4 mas yr^{-1} and of 9 mas yr^{-1}, respectively. Stars within $r_{\rm PM} = 9$ mas yr^{-1} but otherwise outside the cluster region (beyond 3°) and photometrically not following the cluster isochrone are marked with red crosses. (b) The projected PM distribution along the line connecting the field center and the cluster center. The bump near -35 mas yr^{-1} is due to the cluster, which has a standard deviation of 9 mas yr^{-1} when fitted with a Gaussian function.

though diverging toward the lowest mass end, fit the data better. In particular, the KH locus matches even the "kink" of the turn-around toward low-mass stars near $J \sim 12$ mag. This is understandable because the KH compilation was specifically adjusted to Praesepe.

For stars fainter than the 2MASS sensitivity, we resorted to the PS1 data collected up to January 2012. The luminosity function toward Praesepe does not turn over until $g_{\rm P1} \sim 21.5$ mag, but our data are limited by the sensitivity of the PPMXL dataset at around 21 mag. To avoid spurious detections, only sources which have been measured more than twice in both $g_{\rm P1}$ and $y_{\rm P1}$ bands were included in our analysis. The $g_{\rm P1}$ magnitudes were derived from the SDSS magnitudes (taken from KH) transformed to the PS1 photometric system (Tonry et al. 2012), namely, by $g_{\rm p1} = g_{\rm SDSS} - 0.012 - 0.139\,x$, where $x = (g-r)_{\rm SDSS}$. For the $y_{\rm P1}$ magnitudes, because SDSS has no corresponding y, the transformation from $z_{\rm SDSS}$ was used, $y_{\rm P1} = z_{\rm SDSS} + 0.031 - 0.095\,x$, where x is again $(g-r)_{\rm SDSS}$. Because of this, plus the Paschen absorption, the transformation to $y_{\rm P1}$ (and to $z_{\rm P1}$) has a larger uncertainty than in other bands (Tonry et al. 2012). In the transformation to either $g_{\rm P1}$ or $y_{\rm P1}$, using the quadratic instead of the linear fit makes little difference. Figure 3b plots $g_{\rm P1}$ versus $g_{\rm P1} - y_{\rm P1}$ together with the PS1 track transformed from the KH locus. The corresponding stellar mass labeled in the figure was inferred using the listing in KH (their Table 5) by either the J or $g_{\rm P1}$ magnitude at the distance to the cluster. The faint end of the PS1 data corresponds to roughly 0.1 $M_\odot$. At the bright end, the $g_{\rm P1}$ band observations saturate around $g_{\rm P1} \sim 14$ mag, corresponding to about 0.6 $M_\odot$.

The next round of iteration would narrow the photometric criteria. For the 2MASS/PPMXL sample, photometric candidacy is selected in the J versus $J - K_s$ CMD (1) for stars brighter than $J \sim 12$ mag, from 0.06 mag below to 0.18 mag above the Padova MS; for giants there is no photometric restriction, i.e., only the spatial and kinematic criteria were applied; (2) for fainter stars, from 0.1 mag below to 0.1 mag above the Siess

isochrone. For the PS1/PPMXL sample, the selection range is from 0.15 mag below to 0.4 mag above the KH MS locus transformed to the PS1 system (Tonry et al. 2012). The choice of the cutoff in each case is subjective, but seems to work empirically.

Figure 4 shows the radial density profile of stars following the cluster's isochrone and PM, and within the entire 5° field. One sees that the density decreases monotonically until around 3°, then levels off to that of the field. We conclude therefore that Praesepe has an apparent size of 3° in radius, which at a distance of 170 pc, corresponds to a linear dimension of $\sim$ 18 pc across. This size is relatively large among the 1657 entries with both angular diameter and distance determinations in the open cluster catalog compiled by Diaz et al. (2002)[1], with the majority having diameters of 2–4 pc.

The membership identification is now completed. In our analysis, a classification scheme was found useful. Each star is assigned with a classification code. A star has a code of 1 if it is spatially within the cluster region, 2 if the star satisfies the PM criterion, and 4 if the star follows the isochrone. These codes are set bitwise, i.e., additive. So if a star is located within the cluster region and share the PM with the cluster, its code would be 3 if the photometric criterion is not met, and would be 7 if it also follows the appropriate isochrones in the CMD. A star with a code of 7 is considered a member candidate.

The combination of the 2MASS/PPMXL and the PS1/PPMXL samples contains a total of 1040 stars that satisfy all the criteria of photometry (along the isochrone), kinematics (consistent PMs), and spatial grouping (within a 3° radius). In comparison, there are 168 stars satisfying the identical set of criteria except with radii between 4° and 5° (which happens to have the same sky area as the 3° cluster radius) — these are considered field stars and this number of stars should be subtracted from the cluster region.

[1]Updated to January 2013, available at http://www.astro.iag.usp.br/∼wilton/.

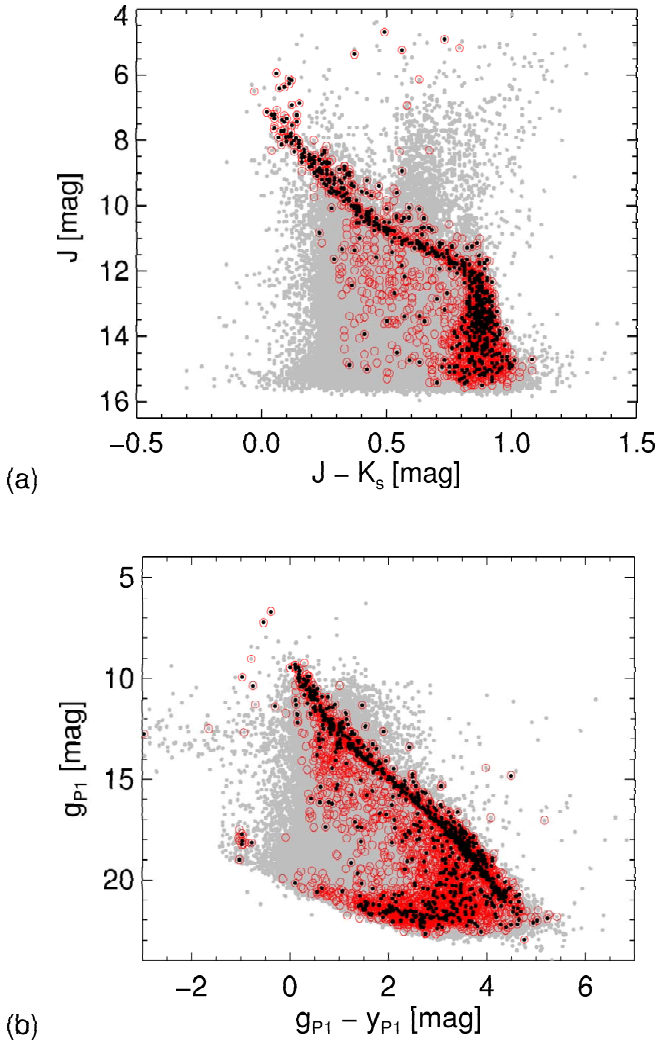

Fig. 3.— (a) The J versus $J - K_s$ CMD for all the stars (gray dots), those within $r_{\rm PM} = 9$ mas yr^{-1} (red crosses) and within $r_{\rm PM} = 4$ mas yr^{-1} (black filled circles). The evolutionary tracks of BCAH, Siess, Padova, and Siess/KeHa Kraus & Hillenbrand (2007) are plotted. Selected stellar mass values are labeled. (b) The $g_{\rm P1}$ versus $g_{\rm P1} - y_{\rm P1}$ CMD. The solid curve is the MS from Kraus & Hillenbrand (2007) transformed to the PS1 system. Symbols are the same as in (a).

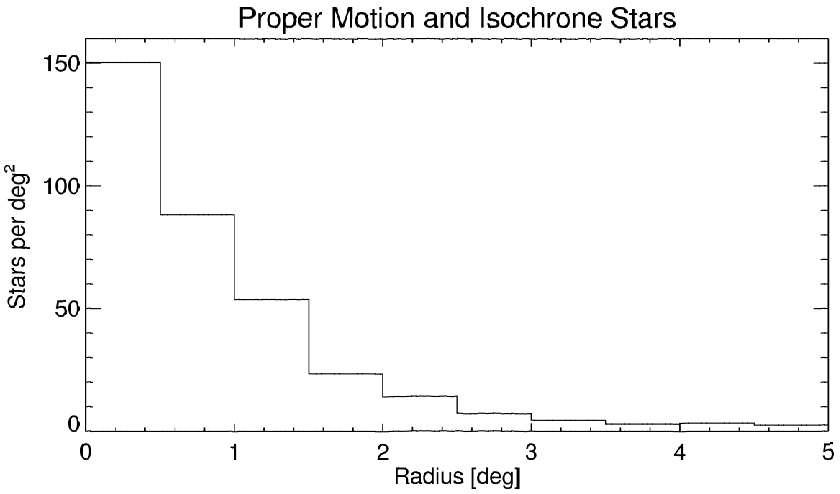

Fig. 4.— The radial density distribution of stars satisfying the isochrone and PM selection, but within the entire 5° field.

So our final list of member candidates contains 1040 stars, among which 872 should be cluster members. Statistically a brighter candidate is more likely to be a true member than a fainter candidate for which the field confusion is higher. If the stringent criterion of $r_{\rm PM} = 4$ mas yr^{-1} had been used instead, the number of candidates would become 547 within 3°, and 33 between 4° and 5°, yielding a net of 514 members within 3°. Table 1 lists the properties of these candidates. The first two columns, (1) and (2), are the identification number and coordinates of a star. Columns (3) and (4) give the PM measurements and errors in R.A. and in declination, all taken from the PPMXL catalog. Subsequent columns, from (5) to (12), list the photometric magnitudes of PS1 $g_{\rm P1}$, $r_{\rm P1}$, $i_{\rm P1}$, $z_{\rm P1}$, and $y_{\rm P1}$, and 2MASS $J_{\rm 2MASS}$, $H_{\rm 2MASS}$, and $K_{\rm 2MASS}$. Column (13) gives the stellar mass. The last column (14) contains 3 kinds of flags (1) flagD to indicate if the candidacy is determined by PS1 data only (flagD=1), by both PS1 and 2MASS (flagD=2), or by 2MASS only (flagD=3), (2) flagK, if the candidate has already been identified in Kraus & Hillenbrand (2007) (flagK=1) or not, and (3) if the candidate has been identified in Boudreault et al. (2010) (flagB=1) or not. The 2MASS and PS1 CMDs of these members are displayed in Figure 5.

4. Discussion

Among the 1040 candidates in Figure 5, 214 were selected by the 2MASS/PPMXL sample only, 83 by PS1/PPMXL only, and 743 by both. The fact that PS1/PPMXL does not find more candidates is, other than the limit at the bright end, because the faintest candidates are very red, $g_{\rm P1} - K_s \approx 7$ mag — in favor of 2MASS detection — and because the PS1/PPMXL data are limited by the brightness limit of the PPMXL dataset. The situation will be improved once the PS1 produces its own PM measurements.

Table 1. Member Candidates of Praesepe

No.	RA	Dec (J2000)	$\mu_{\rm RA}$	err	$\mu_{\rm Dec}$	err	$g_{\rm P1}$	e$g_{\rm P1}$	$r_{\rm P1}$	e$r_{\rm P1}$	$i_{\rm P1}$	e$i_{\rm P1}$	$z_{\rm P1}$	e$z_{\rm P1}$	$y_{\rm P1}$	e$y_{\rm P1}$	J	eJ	H	eH	K	eK	Mass	Flags
		[deg]	mas yr^{-1}		mas yr^{-1}		[mag]		[mag]		[mag]		[mag]		[mag]		[mag]		[mag]		[mag]		$M_\odot$	DKB
(1)		(2)	(3)		(4)		(5)		(6)		(7)		(8)		(9)		(10)		(11)		(12)		(13)	(14)
1	130.449560	20.389607	-38.8	5.6	-14.8	5.6	20.68	0.03	19.39	0.02	18.16	0.04	16.79	0.00	16.40	0.01	15.08	0.04	14.54	0.05	14.23	0.06	0.17	2 1 1
2	130.239570	20.478164	-41.4	5.6	-7.7	5.6	20.64	0.05	19.40	0.02	17.63	0.01	16.85	0.00	16.45	0.01	15.09	0.03	14.56	0.06	14.31	0.08	0.17	2 1 0
3	130.317860	20.815221	-42.5	5.6	-17.7	5.6	21.37	0.06	19.91	0.02	17.96	0.01	17.09	0.00	16.68	0.01	15.36	0.05	14.63	0.05	14.48	0.09	0.12	2 1 1
4	130.348710	20.939491	-41.9	5.6	-19.9	5.6	20.91	0.04	19.66	0.02	17.84	0.01	17.01	0.01	16.62	0.01	15.33	0.05	14.71	0.06	14.46	0.08	0.16	2 1 1
5	130.430800	21.497311	-34.8	5.5	-16.5	5.5	20.71	0.04	19.29	0.01	17.43	0.01	16.49	0.00	16.05	0.00	14.71	0.03	14.06	0.04	13.63	0.04	0.20	2 1 1

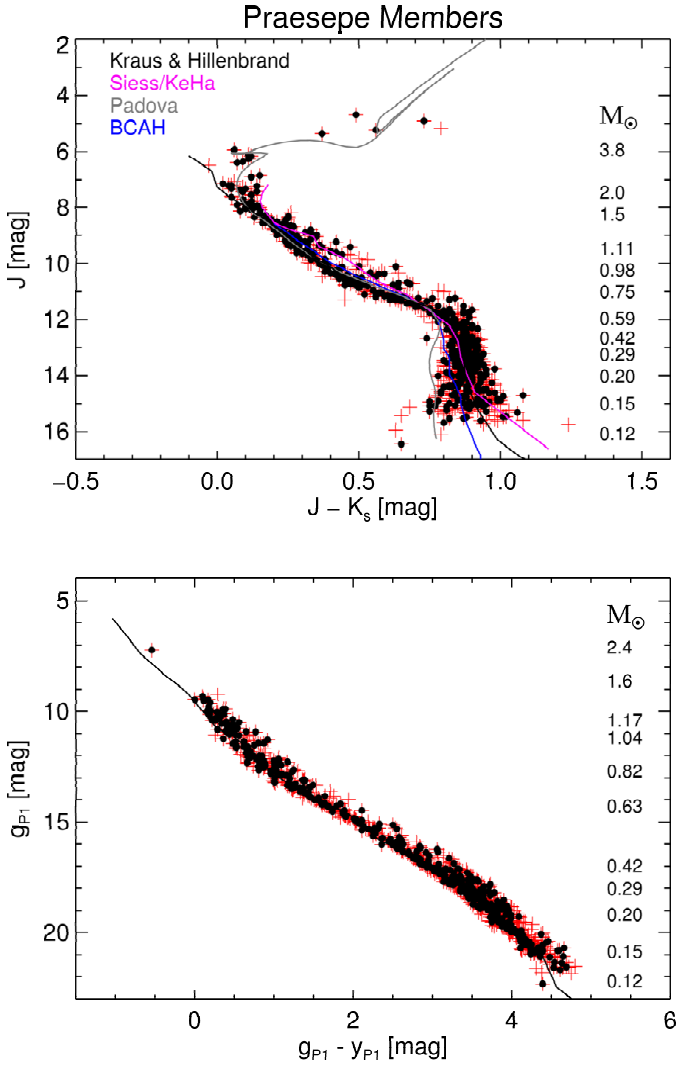

Fig. 5.— Member candidates in Praesepe, selected on the basis of position, proper motion, and magnitude/color. (a) The J versus $J - K_s$ CMD, together with the models by BCAH, Siess, Padova, and Siess/KeHa (Kraus & Hillenbrand 2007). Selected stellar mass values are labeled. (b) The $g_{\rm P1}$ versus $g_{\rm P1} - y_{\rm P1}$ CMD for members. The solid curve is the MS from Kraus & Hillenbrand (2007) transformed to the PS1 system. The red crosses in each panel represent stars within $r_{\rm PM} = 9$ mas yr^{-1} and black dots within $r_{\rm PM} = 4$ mas yr^{-1} of the cluster's mean PM.

4.1. Newly Identified Member Candidates

Our member candidates have been selected as grouping in five out of six dimensional parameters, less only the radial velocity measurements. Among our member candidates, 887 coincide with those by Kraus & Hillenbrand (2007), and 567 with those by Boudreault et al. (2012). Many of our candidates missed by Boudreault et al. (2012) are located in the UKIDSS survey gap. Membership identification by photometry alone, e.g., by González-García et al. (2006) and Boudreault et al. (2010), is vulnerable to significant contamination by field stars, so reliable membership could be secured for bright stars only. To illustrate, the entire PS1/PPMXL sample contains 320,312 stars. There would have been 2445 candidates if only photometric and positional criteria are set, but the number reduces drastically to 826 if the additional $r_{\rm PM} \leq 9$ mas yr^{-1} criterion is imposed.

A few candidates identified in previous works did not pass our PM selection. For example, stars J083850.6+192317 and J084108.0+1914901, listed by González-García et al. (2006) as members on the basis of optical and infrared photometry, have PMs ($\mu_{\rm RA} = 197.5$ mas yr^{-1} and $\mu_{\rm Dec} = 79.6$ mas yr^{-1} for J083850.6+192317, and $\mu_{\rm RA} = -58.4$ mas yr^{-1} and $\mu_{\rm Dec} = 24.9$ mas yr^{-1} for J084108.0+1914901) inconsistent with being part of the Praesepe cluster. Another highly probable member identified by González-García et al. (2006), J084039.3+192840, already refuted by Boudreault et al. (2010) because of its $(I_c - K_s)$ color, is indeed not in our candidate list. We note that our member list includes the two stars recently reported by Quinn et al. (2012), BD+20 2184 (their Pr 0201) and 2MASS J08421149+1916373 (Pr 0211), to host extrasolar planets — first discovery in an open cluster if the lower mass limits estimated from the radial velocity measurements are accepted as being substellar. Their PPMXL measurements are $\mu_{\rm RA} = -36.0 \pm 1.3$ mas yr^{-1} and $\mu_{\rm Dec} = -16.9 \pm 1.3$ mas yr^{-1} for Pr 0201, and $\mu_{\rm RA} = -37.5 \pm 2.2$ mas yr^{-1} and $\mu_{\rm Dec} = -9.8 \pm 2.2$ mas yr^{-1} for Pr 0211. Both stars were

also classified as members by Kraus & Hillenbrand (2007).

4.2. Comparison with Evolutionary Models

Our member list is now ready to confront with stellar evolution models. We will present some practicality when using these models. The Padova isochrones (PARSEC) and their derivatives, including the conversion to colors and magnitudes to facilitate comparison with observations, are available online[2]. The Siess models are also available online, through an isochrone browser[3], with a selection of stellar mass from 0.1 to 7 $M_{\odot}$ and a variety of metallicity values. There are two choices to convert from the effective temperature to observed colors: by the the conversion in Siess et al. (1997) (optical bands only) or by Kenyon & Hartmann (1995) (optical and NIR bands). The one by Kenyon & Hartmann (1995) (KeHa) is a compilation of bolometric corrections (BC) and colors for an effective temperature to compute from the model luminosity to an absolute magnitude, and then to a particular wavelength band. The Padova interface provides transformation to a variety of filter systems, whereas the Siess conversion assumes the Cousin system.

Figure 6a compares the luminosity and the effective temperature computed with the Padova and Siess models, for an age of 900 Myr and metallicity of Z=0.02. The Padova track is systematically fainter, and becomes progressively bluer toward the lower MS, than the Siess track. But even with the same Siess model, the results from the two conversions, shown in Figure 6b, give very similar $V - I_c$ colors or the BC at high temperatures, but diverge below $\log T_{eff} \sim 3.65$. Figure 6c shows the V versus $V - I_c$ CMDs of Padova, Siess with the Siess conversion (Siess/Siess), and Siess with the KeHa conversion (Siess/KeHa).

---

[2]http://stev.oapd.inaf.it/cgi-bin/cmd

[3]http://www.astro.ulb.ac.be/∼siess/WWWTools/Isochrones

The Padova locus is the bluest. Between the two Siess tracks, the Siess/KeHa locus is brighter than Siess/Siess, because the divergence at low temperatures is in such a way that given the same $V - I_c$, the corresponding BC of Siess/KeHa is always larger, resulting in a smaller M_V or a brighter luminosity. Figure 6d shows the comparison of J versus $J - K_s$ isochrones of 890 Myr and the Praesepe metallicity (Fe/H=0.11 ± 0.03, Reglero & Fabregat 1991). One sees that the Padova track is overall below that of the Siess, i.e., bluer given a luminosity. The lesson prompts a cautious selection of models to compare observations with, and the necessity to acquire reliable stellar parameters near the stellar/substellar boundary to help discriminate among theoretical models.

4.3. Binary Fraction

A binary system with identical component stars would have the brightness of either star overestimated by 0.75 mag. A binary sequence therefore is often seen as a swath up to 0.75 mag above the MS of a star cluster in a CMD. Multiple systems may have even larger magnitude differences. In Praesepe this binary sequence stands out clearly in both the 2MASS and the PS1 CMDs. A distinct binary sequence was already noticed by Kraus & Hillenbrand (2007). Note that the J versus $J - K_s$ MS is characterized by a slanted upper part and turns vertically below the mass of ~ 0.6 $M_\odot$. While the upper MS allows us to gauge the distance (shifting vertically), the vertical segment provides a convenient tool to estimate the reddening of a cluster (shifting horizontally). This, however, also means the J versus $J - K_s$ CMD cannot be used to evaluate the binarity at the lower MS. Instead, the PS1 CMD shows a monotonic MS, so can be used for this purpose.

There is no clear dividing line above the MS to separate binaries from single stars. Figure 7 demonstrates a magnitude difference of 0.5 mag above the MS as the dividing line. In this case, there are 200 stars above the line, or a binary fraction of about 19% of the

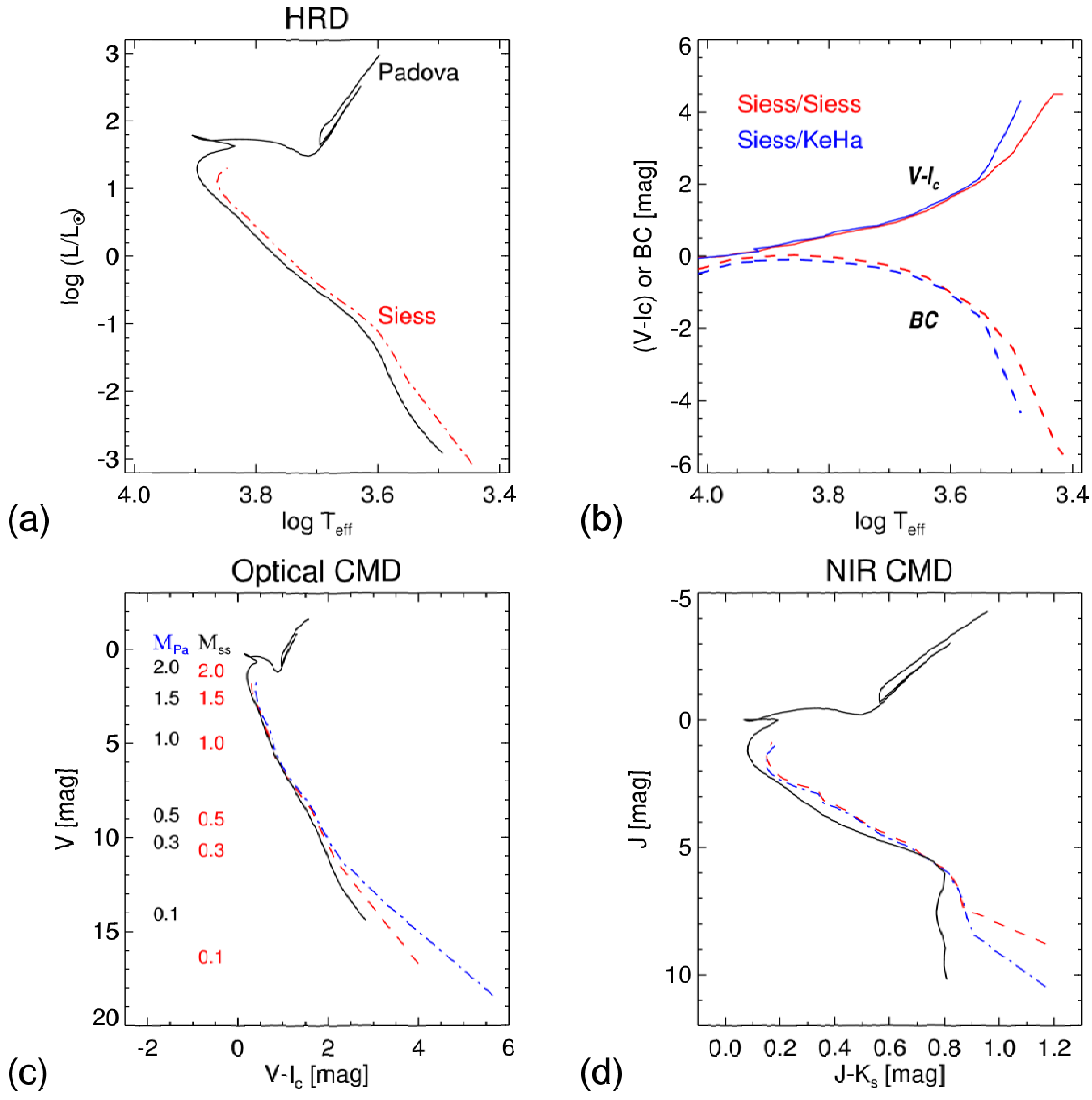

Fig. 6.— (a) Comparison of the Padova and Siess isochrones for 900 Myr and with metallicity [Fe/H]=0.11, or Z=0.02. (b) The $V - I_c$ color and the bolometric correction (BC) of the Siess isochrone (Siess et al. 2000) with the conversions by Siess (Siess et al. 1997) and by Kenyon & Hartmann (1995). (c) The optical V versus $V - I_c$ CMD for the Padova (solid black), Siess/Siess conversion (dashed red), and the Siess/KeHa conversion (dash-dotted blue). (d) The NIR J versus $J - K_s$ CMD.

total 1040 member candidates. If the difference is lower to 0.4 mag or 0.3 mag, the number increases, respectively, to 239 (23%) or 296 (28%). The relatively small increase in the binary fraction is the consequence of a distinct binary sequence of this cluster; that is, the binaries in Praesepe tend to be of similar-mass systems, as noted by, for example, Pinfield et al. (2003). Boudreault et al. (2012) conducted an elaborative analysis on the binarity. Adopting a brightness range from 0.376 to 1.5 mag above the (single star) MS, these authors derived a binary frequency of $23.3 \pm 7.3\%$ for the mass range of 0.45 to 0.2 $M_\odot$, $19.6 \pm 3.8\%$ for 0.2 to 0.1 $M_\odot$, and $25.8 \pm 3.7\%$ for 0.1 to 0.07 $M_\odot$. Given the uncertainties in membership and binarity assignments, our data do not justify division of the sample into different mass bins, and we infer an overall binary fraction of at least 20–30%.

The brightest member in the PS1 sample, with $g_{\rm P1} = 7.23$ mag, is HD 72846, of an A5 spectral type (Fossati et al. 2008). Its parallax of 6.17 ± 0.62 mas (van Leeuwen 2007) indicates membership. The star is clearly above the MS, so notwithstanding the large photometric uncertainties (0.6 mag in all PS1 bands) because of its brightness, the star probably consists of a pair with comparable masses.

4.4. Cluster Mass Function

We now examine the luminosity function and mass function of the cluster. The stellar mass was estimated by the J (if too bright in PS1) or $g_{\rm P1}$ magnitude using the compilation of Kraus & Hillenbrand (2007), and adopting a distance modulus (DM) of 6.15 mag. Figure 8 shows the conversion to the mass, quantized in the model, is fitted by a polynomial function of $g_{\rm P1}$, $M = \sum_{i=1}^{n} a_i \, (g_{\rm P1} - DM)_i$, where n is the order of the polynomial. We found that $n = 6$ shows the best lowest-order fit, with $a_0 = 3.39$, $a_1 = -1.05$, $a_2 = 0.19$, $a_3 = -0.020$, $a_4 = 0.00$, $a_5 = -2.6 \cdot 10^{-5}$, and $a_6 = 2.3 \cdot 10^{-7}$. The lowest mass candidate in our list has a mass of ~ 0.10 $M_\odot$.

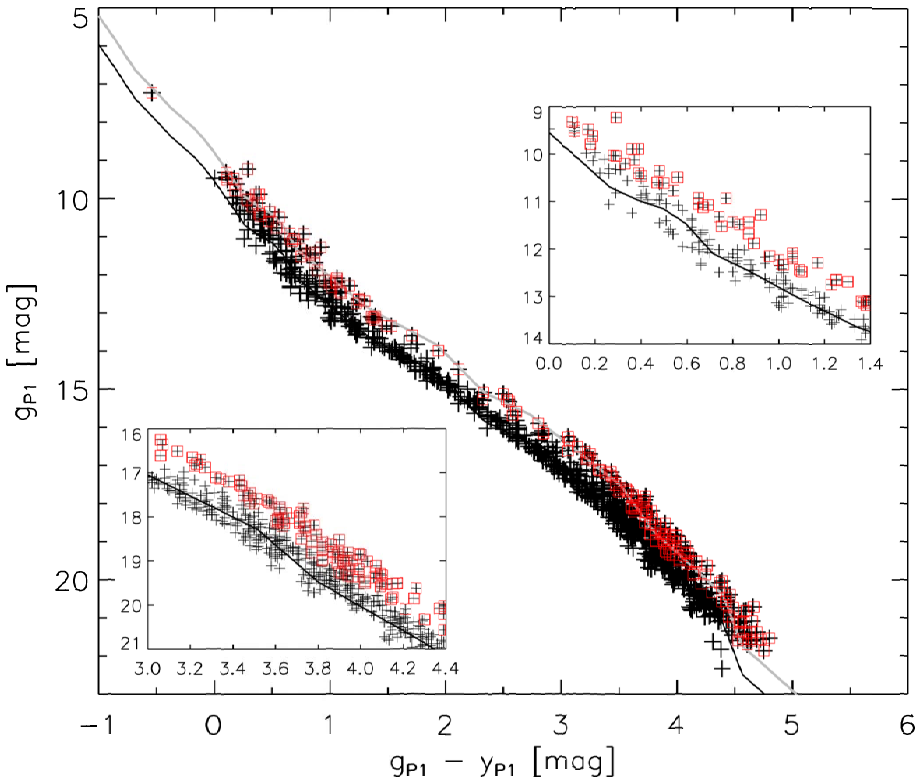

Fig. 7.— Possible binaries diagnosed in the PS1 CMD. The dark solid curve is the MS, whereas the gray curve is the same locus shifted upwards by 0.5 mag as the dividing line to separate binaries (red boxes) from singles (crosses). The two insets show the expanded views of segments of an upper part and a lower part, respectively, for clarity.

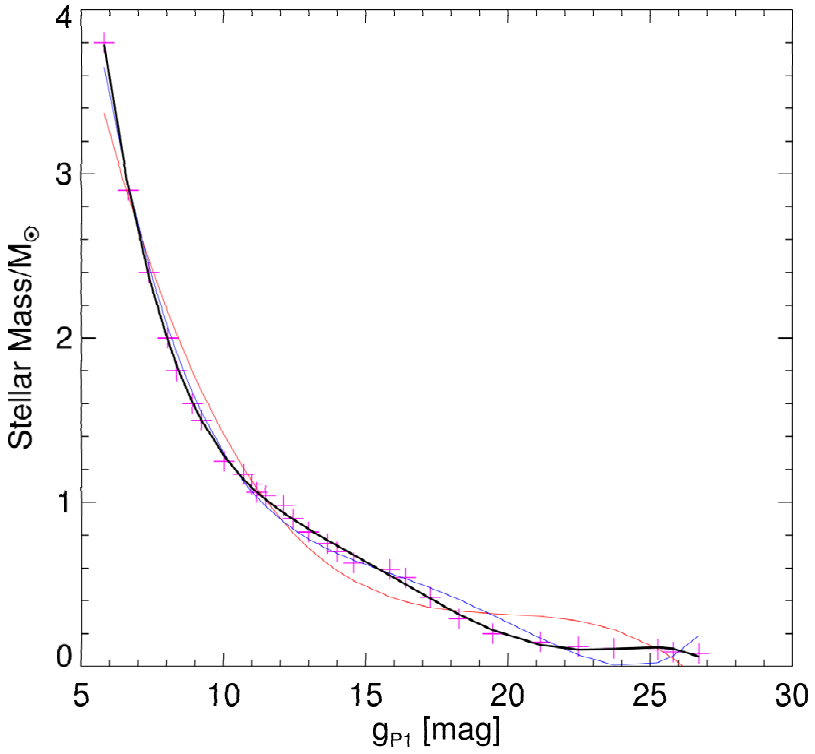

Fig. 8.— The conversion from $g_{\rm P1}$ mag to stellar mass. The horizontal axis is the absolute magnitude of $g_{\rm P1}$, or equivalently the observed $g_{\rm P1}$ mag minus the distance modulus (DM). The cyan triangles represent the compilation of Kraus & Hillenbrand (2007). The gray dashed and dark curves are, respectively, the fifth and sixth order polynomial fit to the data. The sixth order function has been used to compute the stellar mass.

Figure 9a compares the g-band luminosity function of the cluster region (radius $< 3°$) with that of the field (radius 4–5°). Note that fainter than $g \sim 21$ mag, the cluster region (dotted line) is outnumbered by the field (red solid). The luminosity function of the cluster was derived by subtraction of the field contamination. For field stars, we selected the stars satisfying the PM and isochrone criteria, but with angular distance between 4° and 5° from the cluster center (these are code 6 stars). In Figure 9b, the luminosity function of the member candidates listed in Table 1 (represented by the dotted line), is subtracted by that of field stars (the red line). The field distribution is flat, as expected, and contributes only a small correction to the observed luminosity function. The corresponding stellar mass at the distance of Praesepe is labelled on the top of Figure 9b. One sees that the corrected luminosity function (blue solid line) rises beyond the PS1 saturation limit of $g_{\rm P1}$ ∼14–15 mag, and then turns around near $g_{\rm PS1} \sim 18$ mag, or mass ~ 0.3 $M_\odot$ ($\log(M/M_\odot) \approx 0.53$). Derived in a similar manner, the observed and corrected J-band luminosity functions are displayed in Figure 10.

The mass function derived from the J-band (for bright stars) or the corrected g-band luminosity function is shown in Figure 11. Using optical I_c band and NIR J and K_s photometric data, Boudreault et al. (2010) reported a rising mass function in the range from 0.6 $M_\odot$ to 0.1 $M_\odot$ then turning over, in agreement with previous works, e.g., by Hambly et al. (1995b). However, Boudreault et al. (2012), using the UKIDSS data, now adding also the proper motion criterion, obtained an opposite result — a decreasing mass function between 0.6 $M_\odot$ and 0.1 $M_\odot$. The mass function we obtained for the massive part resembles those of the disk population (Chabrier 2005) and of the young Trapezium cluster (Muench et al. 2002), but shows a deficit of the lowest mass population ($\lesssim 0.3$ $M_\odot$), especially so in comparison with that of the Trapezium.

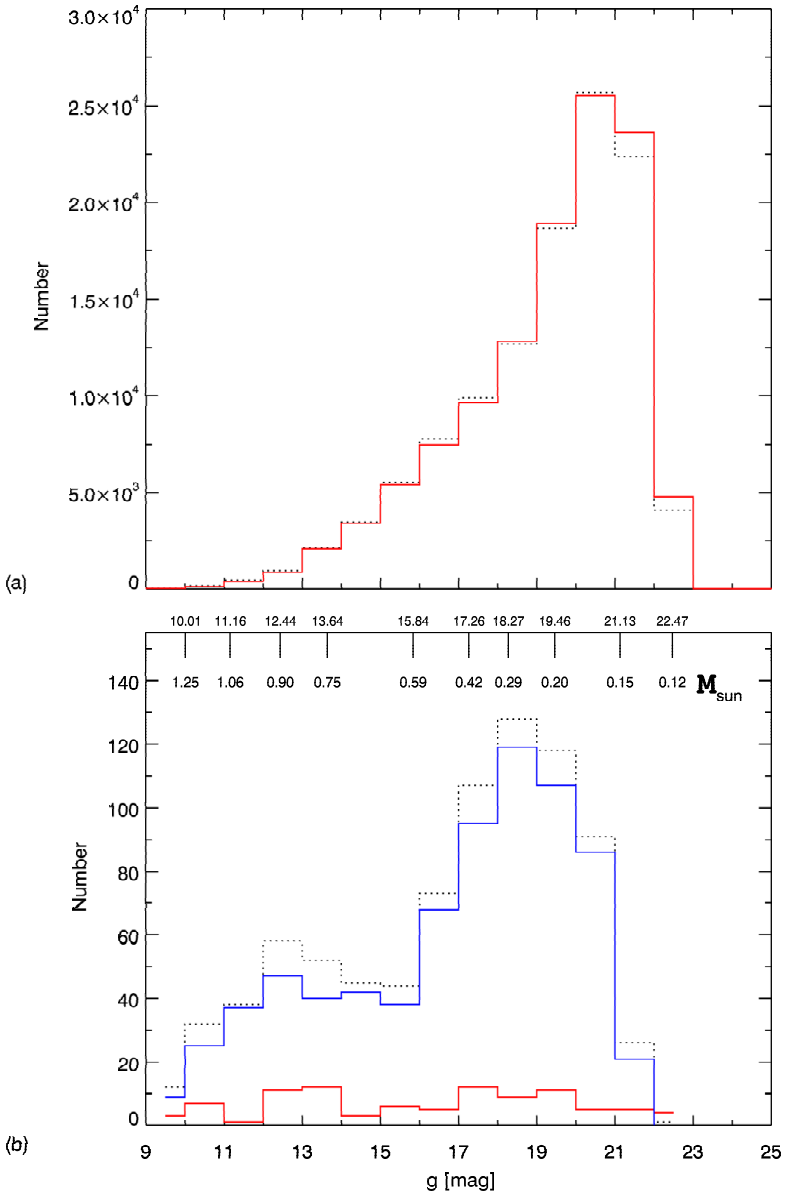

Fig. 9.— (a) The $g_{\rm P1}$ luminosity functions of all the stars within 3° cluster radius (dotted line) and between 4 to 5° radius (solid line). (b) The observed $g_{\rm P1}$ luminosity function of member candidates (dotted line) and that of the field population with the same photometric and PM selection criteria (red lower solid line). The blue solid line shows the corrected (observed subtracts the field) luminosity function. The corresponding stellar mass computed from the $g_{\rm P1}$ magnitude is labeled at the top in unit of the solar mass.

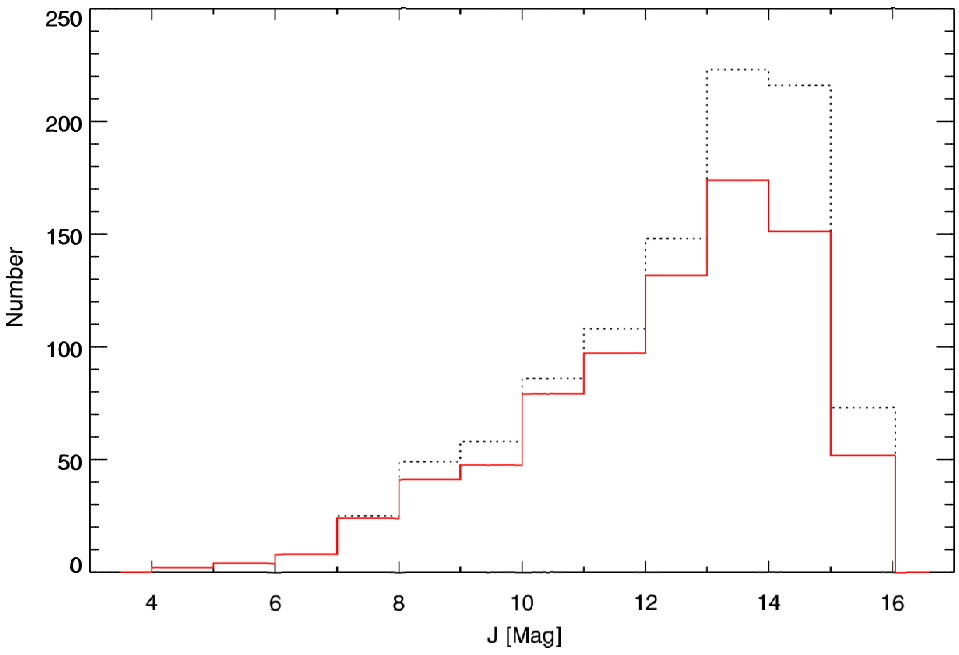

Fig. 10.— The observed (dotted line) and corrected (solid line) J-band luminosity functions of the member candidates in Praesepe.

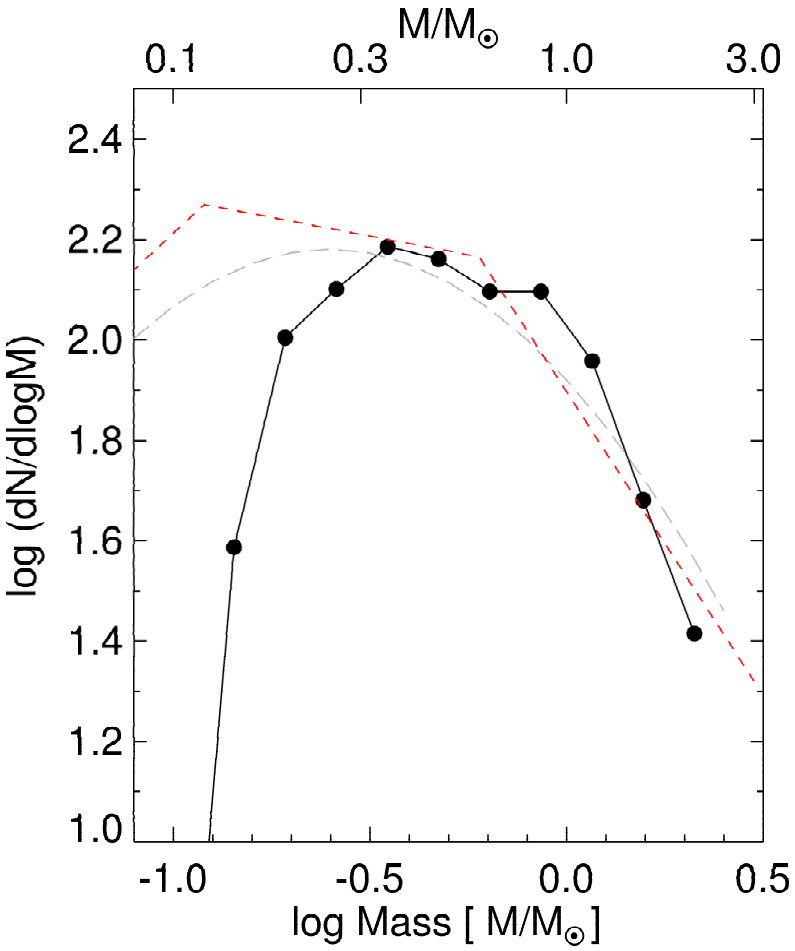

Fig. 11.— The mass function of Praesepe (solid line). Also shown are those by Chabrier (2005) for the disk population (long-dashed line) and by Muench et al. (2002) for the Trapezium cluster (dashed line), each shifted vertically for display clarity.

4.4.1. Spatial Distribution of Members

Galactic open clusters are found to have elongated shape, even for the youngest ones of only a couple million years old (Chen, Chen, & Shu 2004). The stellar distribution in a stellar system at birth must reflect the structure and formation conditions in the parental molecular cloud. Encounters among member stars then circularize the core of the cluster. Mass segregation occurs as energy losing massive stars sink to the center, whereas lower-mass members gain energies and occupy a larger volume in space. Some stars may gain sufficient speed so as to escape the system. The lowest mass members are particularly vulnerable to such stellar "evaporation". As the cluster evolves, the internal gravitational pull becomes weaker and external disturbances, such as differential rotation, or tidal force from passing molecular clouds and from the Galactic disk, act together to distort the shape of a cluster and eventually tear it apart. The deformation and tidal stripping are effective even for globular clusters (Chen & Chen 2010).

Figure 12 shows how the stellar mass correlates with the spatial distribution. The radial density profiles have been computed for 4 different mass groups: $M/M_{\odot} \leq 0.2$ (129 stars), $M/M_{\odot}$ =0.2–0.35 (256 stars), $M/M_{\odot}$ =0.35–0.7 (332 stars), and $M/M_{\odot} \geq 0.7$ (323 stars). The top panel shows the observed density profiles, while the bottom panel compares the normalized profiles. Because of the normalization, no correction of the field contamination is necessary. One sees that relatively massive members appear to be centrally concentrated, whereas lower mass members are more scattered spatially. Mass segregation is clearly evidenced.

Mass segregation in Praesepe has been well demonstrated already by Hambly et al. (1995b) and Kraus & Hillenbrand (2007). Our result is consistent with that by Hambly et al. (1995b), who divided the members by m_I brighter than 12 mag (0.85 $M_{\odot}$), between 12 and 15 mag (0.40 $M_{\odot}$), and between 15 to 18 mag (0.15 $M_{\odot}$). If the radial density

distribution shown in Figure 12 is parameterized with an exponential form, $\sigma(r) \propto e^{-\alpha r}$, the least-squared fitting yields $\alpha = 2.21$ for members > 0.7 $M_\odot$, $\alpha = 0.96$ for the mass range 0.35–0.7 $M_\odot$, and $\alpha = 0.42$ for stars 0.2–0.35 $M_\odot$. For the faintest sample, the density distribution is certainly not exponential. Instead, it exhibits a sharp truncation beyond 1°, a probable consequence of stellar evaporation. This further supports the notion of a relative lack of lowest mass stars demonstrated in Figure 11.

Mass segregation is further manifested by the positional and PM distributions of the members, as shown in Figure 13, that relatively higher mass members are concentrated in a smaller volume in space, and have a smaller velocity dispersion than lower-mass stars. The average stellar mass in our sample is $\bar{m} \approx 0.59$ $M_\odot$, close to that for a Miller-Scalo initial mass function. With the total number of members $N = 872$, the total stellar mass in the cluster amounts to at least ~ 520 $M_\odot$. The lowest mass stars, with a declining mass function, do not contribute significantly to the total mass. With a radius $R = 9$ pc, the velocity dispersion of the cluster then would be $v \approx (GN\bar{m}/R)^{1/2} = 0.5$ km s^{-1}, which is noticeably less than the typical value of 1–2 km s^{-1} for Galactic open clusters. At the assumed distance of 170 pc to Praesepe, an intracluster PM dispersion of 1 mas yr^{-1} corresponds to a velocity dispersion of 0.8 km s^{-1}. Our data thus are not precise enough to measure any PM gradient among members.

The evidence is mounting that Praesepe is dissolving. It is spatially extended, with a sparse stellar density. The relatively high fraction of equal mass pairs (and of multiples) may be the consequence of occasional stellar ejection during three-body encounters (Binney & Tremaine 1987). Relevant time scales for a dissolving star cluster include: (1) the dynamical (crossing) time scale, $\tau_{\rm dyn} \approx 2R/v$, (2) the relaxation time, $\tau_{\rm relax} \approx \tau_{\rm dyn}\, 0.1\, N/\ln N$, and (3) the evaporation time, $\tau_{\rm evap} \approx 100\, \tau_{\rm relax}$ (Binney & Tremaine 1987). For Praesepe, these time scales are $\tau_{\rm dyn} = 3.6 \cdot 10^7$ yr, $\tau_{\rm relax} = 4.6 \cdot 10^8$ yr, and $\tau_{\rm evap} = 4.6 \cdot 10^{10}$ yr, respectively.

The lowest-mass members, having an average escape probability (Spitzer 1987) several times of that for the most massive stars, are particularly susceptible to ejection. At an age of 890 Myr, the Praesepe cluster therefore is almost fully relaxed, and tidal stripping has occurred, as suggested by Kraus & Hillenbrand (2007), with the lowest mass members being witnessed to escape from the system.

One final note about our study is the possibility of pre-main sequence (PMS) population in the cluster, something usually overlooked for an intermediate-age cluster like Praesepe. The Padova track for example indicates that the lowest-mass stars in our sample, ~ 0.11 $M_{\odot}$, are still in the PMS stage. Figure 14 plots the PMS time span, defined as the time lapse from the stellar birthline to the zero-age main sequence, versus stellar mass, computed with the Yale Stellar Evolution Code for solar abundances (Jung & Kim 2007). While a one-solar mass star takes 36 Myr to complete the PMS evolution, it takes proportionally longer for lower mass stars, reaching the maximum 1.27 Gyr for 0.11 $M_{\odot}$. Praesepe thus should be populated with PMS stars at the hydrogen burning limit or BDs. If so, this requires a revised range of magnitudes and colors for membership selection. Such a modification does not affect the normalized density distribution — so our conclusion of the tidal stripping should be robust — but conceivably should alter the member list, and thereby also the derived mass function, etc. At the faint magnitude end, the bottleneck of membership selection for very faint objects remains the sensitivity of the PM measurements. Once the PS1 completes its survey at the end of 2013, increasing the photometric depth and the stellar PM baseline to 3.5 years, we expect to secure member lists for nearby star clusters well into the substellar regime.

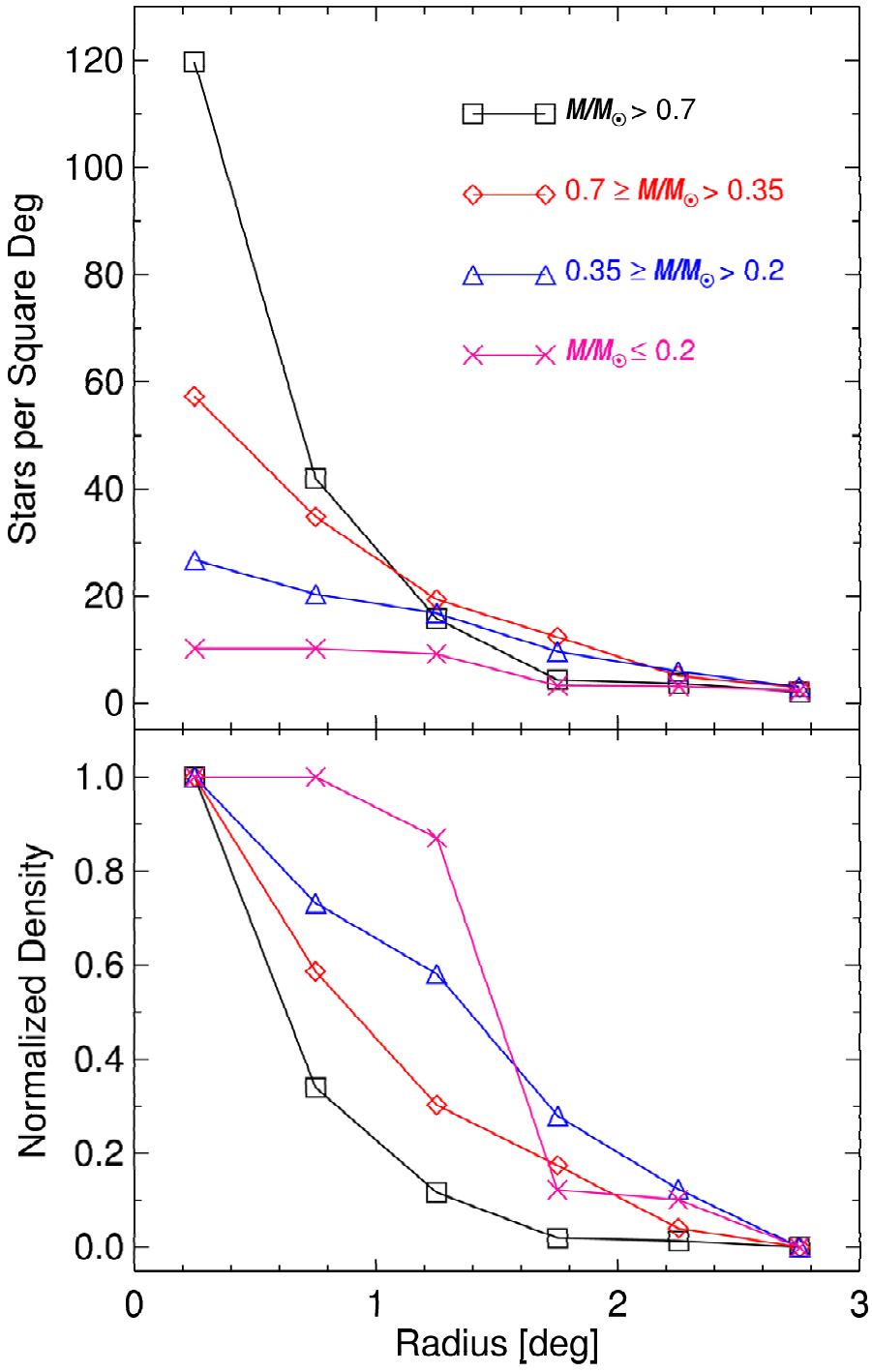
Stars per Square Deg
120
100
80
60
40
20
0
M/M⊙ > 0.7
0.7 ≥ M/M⊙ > 0.35
0.35 ≥ M/M⊙ > 0.2
M/M⊙ ≤ 0.2
Normalized Density
1.0
0.8
0.6
0.4
0.2
0.0
0
1
2
3
Radius [deg]

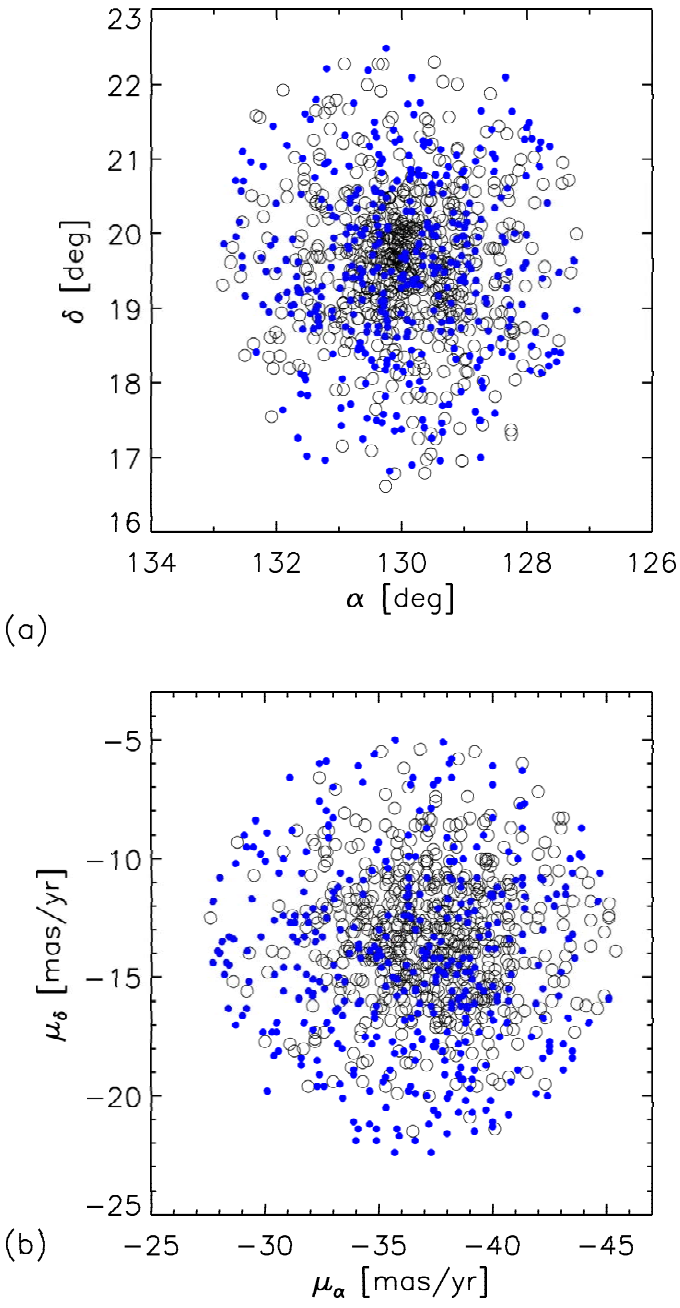

Fig. 13.— (a) Positional distributions of stars more massive (open circles) and less massive (solid circles) than 0.35 $M_{\odot}$. (B) Proper motion distributions for the same two mass groups of members.

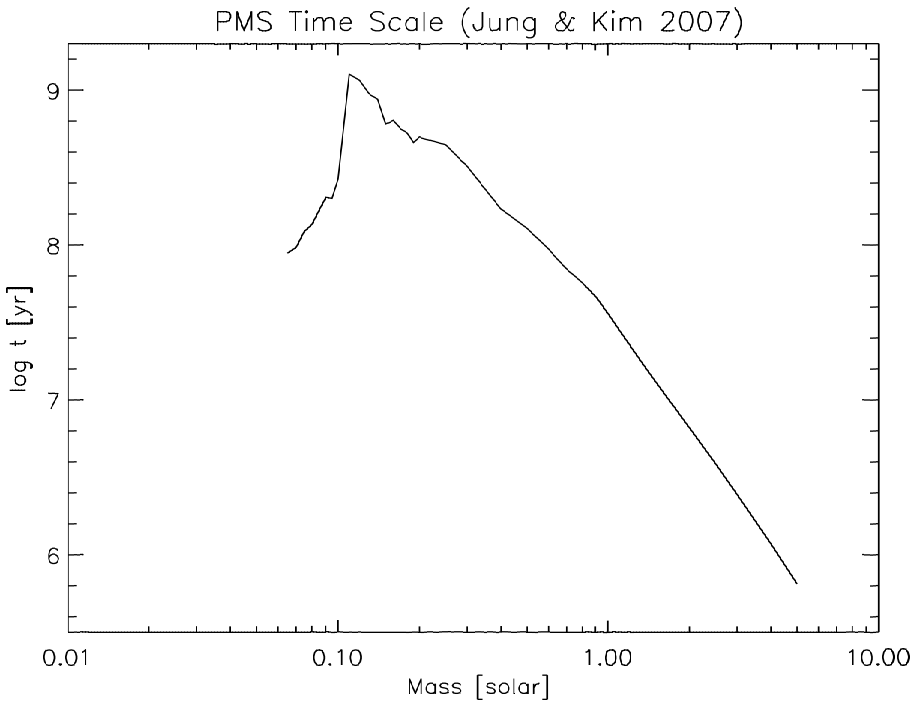

Fig. 14.— The pre-main sequence time scale versus stellar mass (Jung & Kim 2007).

5. Summary

Using 2MASS, PPMXL and Pan-STARRS data, we have identified a total of 1040 member candidates in Praesepe, 872 of which are highly probable members, down to the stellar limit of about 0.1 solar masses. For members more massive than 0.6 $M_{\odot}$, the Padova isochrone works well, but it fails to fit fainter members. Some candidates found in previous photometric studies have proper motions inconsistent with membership. The binary frequency of Praesepe members is about 20-30%, with a relatively high occurrence of similar mass pairs. The mass function is consistent with that of the disk population, but with a deficit of stars less massive than 0.3 $M_{\odot}$. Members show a clear evidence of mass segregation, with the lowest mass population being evaporated from the system.

This project is financially supported partially by the grant NSC101-2628-M-008-002.

The Pan-STARRS1 Surveys (PS1) have been made possible through contributions of the Institute for Astronomy, the University of Hawaii, the Pan-STARRS Project Office, the Max-Planck Society and its participating institutes, the Max Planck Institute for Astronomy, Heidelberg and the Max Planck Institute for Extraterrestrial Physics, Garching, The Johns Hopkins University, Durham University, the University of Edinburgh, Queen's University Belfast, the Harvard-Smithsonian Center for Astrophysics, the Las Cumbres Observatory Global Telescope Network Incorporated, the National Central University of Taiwan, the Space Telescope Science Institute, the National Aeronautics and Space Administration under Grant No. NNX08AR22G issued through the Planetary Science Division of the NASA Science Mission Directorate, the National Science Foundation under Grant No. AST-1238877, and the University of Maryland.

REFERENCES

Abazajian, K. N., Adelman-McCarthy, J. K., Agüeros, M. A., et al. 2009, ApJS, 182, 543

Adams, J. D., Stauffer, J. R., Skrutskie, M. F., et al. 2002, AJ, 124, 1570

Baraffe, I., Chabrier, G., Allard, F., & Hauschildt, P. H. 1998, A&A, 337, 403

Binney, J., & Tremaine, S. 1987, "Galactic Dynamics", Princeton, NJ, Princeton University Press, 1987

Boudreault, S., Bailer-Jones, C. A. L., Goldman, B., Henning, T., & Caballero, J. A. 2010, A&A, 510, A27

Boudreault, S., Lodieu, N., Deacon, N. R., & Hambly, N. C. 2012, MNRAS, 426, 3419

Bouvier, J., Kendall, T., Meeus, G., et al. 2008, A&A, 481, 661

Chabrier, G. 2005, The Initial Mass Function 50 Years Later, Astrophy. & Space Sci. Lib., 327, 41

Chappelle, R. J., Pinfield, D. J., Steele, I. A., Dobbie, P. D., & Magazzù, A. 2005, MNRAS, 361, 1323

Chen, W. P., Chen, C. W., & Shu, C. G. 2004, AJ, 128, 2306

Chen, C. W., & Chen, W. P. 2010, ApJ, 721, 1790

Cutri, R. M., Skrutskie, M. F., van Dyk, S., et al. 2003, VizieR Online Data Catalog, 2246, 0

de La Fuente Marcos, R., & de La Fuente Marcos, C. 2000, Ap&SS, 271, 127

Dias, W. et al. 2002, A&A, 389, 871

Eggen, O. J. 1960, MNRAS, 120, 540

Fossati, L., et al. 2008, A&A, 483, 891

Girard, T. M., Grundy, W. M., López, C. E., & van Altena, W. F. 1989, AJ, 98, 227

González-García, B. M., Zapatero Osorio, M. R., Béjar, V. J. S., et al. 2006, A&A, 460, 799

Hambly, N. C., Steele, I. A., Hawkins, M. R. S., & Jameson, R. F. 1995, A&AS, 109, 29

Hambly, N. C., Steele, I. A., Hawkins, M. R. S., & Jameson, R. F. 1995, MNRAS, 273, 505

Hodapp, K.W., Siegmund,W. A., Kaiser, N., et al. 2004, Proc. SPIE, 5489, 667

Høg, E., Fabricius, C., Makarov, V. V., et al. 2000, A&A, 355, L27

Jones, B. F., & Cudworth, K. 1983, AJ, 88, 215

Jones, B. F., & Stauffer, J. R. 1991, AJ, 102, 1080

Jung, Y. K., & Kim, Y.-C. 2007, J. of Astron. and Sp. Sci., 24, 1

Kaiser, N., et al. 2010, Proc. SPIE, 7733, 12

Klein-Wassink, W. J. 1927, Pub. of the Kapteyn Astron. Laboratory Groningen, 41, 1

Kenyon, S. J., & Hartmann, L. 1995, ApJS, 101, 117

Kraus, A. L., & Hillenbrand, L. A. 2007, AJ, 134, 2340

Loktin, A. V., & Beshenov, G. V. 2003, Astron. Rep., 47, 6

Marigo, P., Girardi, L., Bressan, A., et al. 2008, A&A, 482, 883

Mermilliod, J.-C., Weis, E. W., Duquennoy, A., & Mayor, M. 1990, A&A, 235, 114

Muench, A. A., Lada, E. A., Lada, C. J., & Alves, J. 2002, ApJ, 573, 366

Pinfield, D. J., Hodgkin, S. T., Jameson, R. F., Cossburn, M. R., & von Hippel, T. 1997, MNRAS, 287, 180

Pinfield, D. J., Dobbie, P. D., Jameson, R. F., et al. 2003, MNRAS, 342, 1241

Quinn, S. N., White, R. J., Latham, D. W., et al. 2012, ApJ, 756, L33

Reglero, V., & Fabregat, J. 1991, A&AS, 90, 25

Roeser, S., Demleitner, M., & Schilbach, E. 2010, AJ, 139, 2440

Siess, L., Forestini, M., & Dougados, C. 1997, A&A, 324, 556

Siess, L., Dufour, E., & Forestini, M. 2000, A&A, 358, 593

Spitzer, L., Jr., & Shull, J. M. 1975, ApJ, 201, 773

Spitzer, L. 1987, "Dynamical Evolution of Globular Clusters", Princeton, NJ, Princeton University Press, 1987

Taylor, B. J. 2006, AJ, 132, 2453

Tonry, J. L., Burke, B. E., Isani, S., Onaka, P. M., & Cooper, M. J. 2008, Proc. SPIE, 7021, 9

Tonry, J. L., Stubbs, C. W., Lykke, K. R., et al. 2012, ApJ, 750, 99

van Leeuwen, F. 2007, A&A, 474, 653

This manuscript was prepared with the AAS LaTeX macros v5.2.